Advances in Science and Technology Research Journal

Advances in Science and Technology Research Journal, 2025, 19(9), 214–236
https://doi.org/10.12913/22998624/207125
ISSN 2299-8624, License CC-BY 4.0

Received: 2025.03.04
Accepted: 2025.07.15
Published: 2025.08.01

The effect of grain size on the mechanical properties and abrasion resistance of high-strength Hardox Extreme steel

Martyna Zemlik[1*], Beata Białobrzeska[1], Łukasz Konat[1]

[1] Department of Vehicle Engineering, Faculty of Mechanical Engineering, Wrocław University of Science and Technology, ul. Wybrzeże Wyspiańskiego 27, 50-370 Wrocław, Poland
* Corresponding author's e-mail: martyna.zemlik@pwr.edu.pl

ABSTRACT

This paper presents the results of an analysis of the influence of prior austenite grain (PAGS) size on the strength and ductility of Hardox Extreme steel, with particular emphasis on impact toughness and abrasion resistance under loose abrasive conditions. According to the manufacturer, Hardox Extreme steel in its delivered state is characterized by a minimum tensile strength of 2000 MPa and a hardness 650–700 HBW. To conduct the analysis, Hardox Extreme steel underwent heat treatment, including austenitization at temperatures ranging from 850 to 1200 °C. The mechanical property tests were supplemented with microscopic analysis using stereoscopic, light (LM), and scanning electron microscopy (SEM) to evaluate microstructural properties. Fractographic studies were also carried out to identify the fracture characteristics observed during impact tests. Additionally, surface analyses after abrasion tests were performed to determine the micromechanisms of wear. Quantitative metallography techniques and statistical tools were employed to evaluate the prior austenite grain size and its distribution across various austenitization temperatures. The final section discusses the results in relation to existing literature and presents scientific and practical conclusions.

Keywords: Hardox Extreme, grain size, microstructure, mechanical properties, abrasion resistance.

INTRODUCTION

Modern industrial demands, especially in the mining and construction sectors, present engineers with the challenge of designing steels that combine high strength and abrasion resistance with good ductility. Among these materials, Hardox Extreme steel occupies a prominent position, boasting a tensile strength of at least 2000 MPa and hardness exceeding 650 HBW. This steel belongs to the group of martensitic steels with enhanced wear resistance and is considered one of the hardest wear-resistant steels in the world, according to its manufacturer [1–3]. Material datasheets provide its chemical composition and carbon equivalent, while mechanical properties are limited to hardness values. Therefore, determining additional parameters is essential, especially since welding techniques intended for joining Hardox Extreme sheets cause significant microstructural changes in the heat-affected zone [4]. Based on laboratory and field research results [5], it is clear meeting operational requirements depends on a range of microstructural, strength, and plastic properties. Evaluating the microstructural properties of Hardox Extreme steel is particularly important because its mechanical properties − such as strength, ductility, impact toughness, and abrasion resistance − are closely tied to the microstructure obtained after thermo-mechanical treatments. Microstructural morphology can be assessed in various ways, but grain size, specifically prior austenite grain size (PAGS), has a pronounced effect on the mentioned parameters. It should be noted that specific microstructural parameters (e.g., the presence of secondary phases or PAGS) may lead to variations in wear behavior, even among materials with similar hardness ranges as declared by manufacturers [6–9]. In certain cases, surface hardening (altering the

type and morphology of the microstructure) can positively affect brittleness, leading to an increase in fracture energy above the commonly accepted toughness threshold of 27 J (35 J/cm^2) [10–13]. This behavior can be advantageous when using steel in impact-wear conditions.

The mechanical properties of metallic materials can be enhanced through solution hardening, precipitation strengthening, dispersion strengthening, plastic deformation (work hardening), and heat treatment. However, one of the fundamental methods for improving the mechanical properties of steel is grain boundary strengthening. According to Hall-Petch equation, at ambient temperature, increasing the yield strength can be linked to refining (reducing) the grain size of the microstructure [14–17]. This mechanism is based on the theory that grain boundaries act as significant obstacles to dislocation motion due to changes in crystallographic lattice orientation and the formation of atomic mismatch zones. In larger grains, dislocation pile-ups at grain boundaries generate stresses capable of overcoming the energy barrier, enabling further atomic diffusion.

In addition to improving mechanical properties, a smaller PAGS can also influence the hardening capability of martensitic steels by altering dislocation density [16, 18]. The PAGS determines the properties of steel in both annealed and heat-treated states. Steels with microstructures composed of fine-lath martensite (such as the previously discussed Hardox grades, as well as TBL and XAR) exhibit tensile strength R_m in the range of 1300–2500 MPa. The organization of such a microstructure relative to PAG can be represented hierarchically. During cooling of low- and medium-carbon steels, austenite grains divide into packets along habit planes, forming high-angle boundaries (Fig. 1). These packets consist of blocks with approximately aligned crystallographic orientations (low-angle boundaries), which are further divided into laths that form the crystallographic unit of martensite. According to the Kurdjumov-Sachs theory, 24 crystallographic orientation variants of laths are possible [19], as during shearing, one of the six slip planes {110} of martensite aligns parallel to one of the four slip planes {111} of austenite [20]. Research indicates that the sizes of both packets and blocks contribute to improved strength and fracture resistance [14, 21]. Similar conclusions were drawn in [22], where it was shown that packet boundaries can serve as significant obstacles to dislocation motion, and microstructural refinement enhances the nominal yield strength.

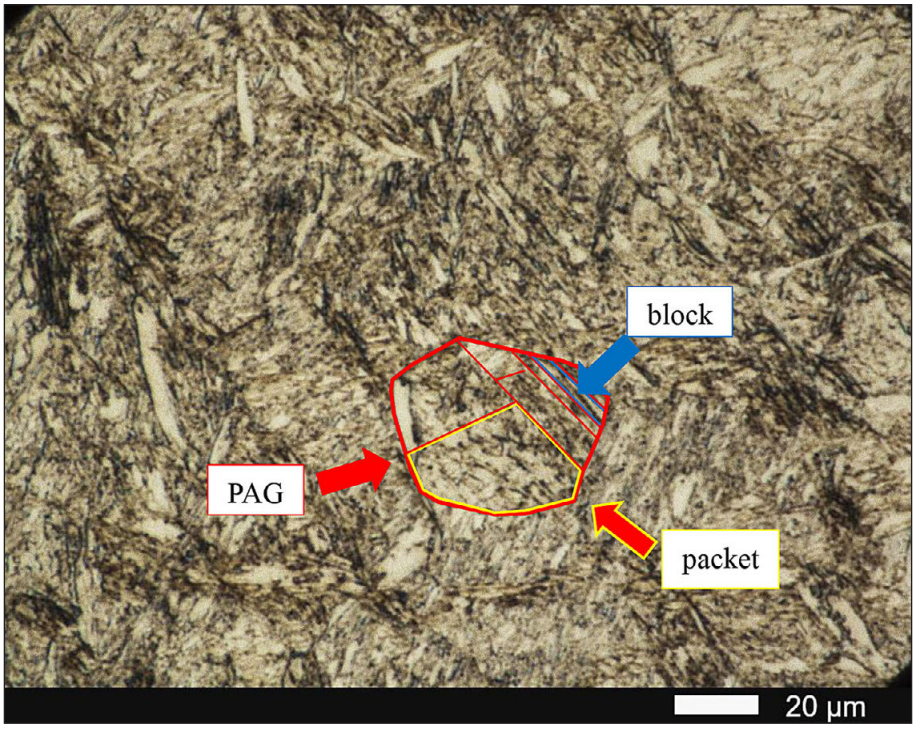

Figure 1. The microstructure of Hardox Extreme steel, with its hierarchical division of martensite relative to prior austenite grain (PAG) boundaries, into packets and blocks, is shown schematically. LM, etched with reagent 3 according to ASTM E407

It is important to note that in low-carbon martensitic steels, PAGS has a negligible effect on hardness and tensile strength R_m, but a significant influence on dynamic loading conditions. Thus, impact wear resistance is particularly susceptible to degradation. According to [23], an increase in grain size in Hardox 450 steel to 123.7 µm results in a reduction in tensile strength R_m to 1382 MPa, representing 96% of the value achieved in its as-delivered state. In comparison, impact toughness decreases from KCV = 70.3 J/cm^2 to KCV = 19.0 J/cm^2, which falls below the material's accepted brittleness threshold of 35 J/cm^2 [10]. Maintaining high plasticity parameters is critical to ensuring the durability of components such as chutes, hoppers, conveyors, and plowshares exposed to dynamic loading from material mass.

Fine-grained steels, characterized by smaller austenite grains, enable the use of higher finish temperatures during hot plastic deformation. Furthermore, they expand the austenitization temperature range during quenching. The fine-grained microstructure results in improved mechanical and operational properties in normalized, quenched, and heat-treated steels [24]. At room temperature, hardness, yield strength, tensile strength, and impact toughness increase with decreasing grain size. The degree of grain refinement (microstructure) is also associated with stresses occurring in the material subjected to heat treatment. In this context, Type II stresses (macrostresses) arise from the heterogeneous structure of metallic bodies composed of grains and grain blocks. These stresses influence the anisotropy of elastic and plastic properties, and grain boundaries exhibit dislocation pile-ups and other defects [25]. Given these relationships, it is assumed that austenite grain size should affect the tribological resistance of steel. For example, changes in austenite grain size in the microstructure of Hardox 450 steel influenced the average weight-loss intensity during wear [26], Grain growth in this steel led to increased mass losses, with significant wear associated with the presence of abnormal grains in the microstructure. Microstructures with an average grain size no larger than 40 µm exhibited greater abrasion resistance than those with abnormal grain growth. A similar correlation between weight loss and grain size was reported in [27]. The PAGS in steel may also indirectly affect abrasion resistance. It has been shown that reducing the austenite grain size decreases the size of packets and blocks in the martensitic microstructure, thereby improving its strength and ductility [19, 28–30]. Additionally, susceptibility to cracking under load decreases with the size of individual laths [28, 31].

According to information in [32], steel with a hardness of 500 HB exhibits lower wear rates when its microstructure consists of equiaxed grains with a size of 14 µm. Similar conclusions were drawn in [33–35]. These analogies also apply to Hadfield steel [36], where microstructural refinement increased abrasion resistance by 16.4% compared to the initial state.Given the limited information available in the literature on Hardox Extreme steel, the objective of this study is to analyze the effect of PAGS, shaped during austenitization at temperatures ranging from 850 to 1200 °C, on the hardness, tensile and yield strength, percentage elongation at break, impact toughness, and abrasion resistance of Hardox Extreme steel. The results will be compared with existing literature to enhance the understanding of the mechanisms influencing the material's properties and to provide recommendations for its optimal industrial application The results will be compared with existing literature to better understand the mechanisms governing the properties of this steel.

MATERIALS AND METHODS

Materials

The chemical composition was determined using a spectral technique with a Leco GDS500A glow discharge spectrometer. The test samples, measuring 20 × 20 mm, were cut from a sheet with a thickness of 10 mm. For preliminary preparation, the surfaces were ground using 320-grit zirconium sandpaper. The analysis was conducted on the cross-sectional surface. To achieve ionization of the inert gas, the following settings were used: voltage of 1250 V, current of 45 mA, and high-purity argon (99.999%). The results are presented as the arithmetic mean of no fewer than five measurements. The chemical composition of the analyzed material is presented in Table 1.

Heat treatment operations were carried out in gas-tight chamber furnaces (FCF 12SHM/R, Czylok) with a protective atmosphere of 99.95% argon. The quenching bath used synthetic quenching oil (Durixol W72) with a kinematic viscosity of 21 mm^2/s, preheated to a temperature

Table 1. Chemical composition of Hardox Extreme steel, in wt.%

C	Mn	Si	P	S	Cr	Ni	Mo
0.45	1.00	0.14	0.006	0.000	0.07	0.70	0.07
V	Cu	Al	Ti	Nb	Co	B	Zr
0.008	0.005	0.04	0.003	0.000	0.01	0.0011	0.000

of 50 °C. Detailed heat treatment parameters are provided in Table 2.

Microstructural analysis

Macroscopic observations were conducted using a Nikon AZ100 multifunctional stereoscopic microscope. These observations included fracture surfaces in both the as-delivered state and after heat treatment. Microscopic examinations to assess the microstructure were carried out using a Nikon Eclipse MA200 microscope and a Phenom XL (backscattered electron detector (BSD), 15 kV accelerating voltage). The samples were etched with reagent 3, following ASTM E407. To reveal prior austenite grain boundaries, reagent 79 was used. Surface observations following laboratory abrasion resistance tests and fracture surface analyses were conducted in an unetched condition using a Phenom XL microscope (BSD detector, 15 kV accelerating voltage). These studies were also performed for both the as-delivered and heat-treated states.

A quantitative assessment of PAGS was carried out in selected sample areas using ImageJ software. The cross-sectional areas (a) of 150 randomly chosen grains were measured following the planimetric approach, and the corresponding flat grain diameter (d) was derived as $\sqrt{a}$. Data processing was conducted with Statistica (version 13). Grain size distributions were determined using 12 fixed classes, and the empirical results were compared with theoretical models, including log-normal, exponential, and gamma distributions. The conformity between experimental and theoretical distributions was verified using Pearson's χ^2 test.

Mechanical property testing

Hardness tests were conducted with a Zwick/Roel ZHU 187.5 tester, utilizing the Brinell method in accordance with the ISO 6506-1:2014 standard. A tungsten carbide ball with a diameter of 2.5 mm was used, applying a load of 187.5 kgf (1838.7469 N) for 15 seconds. Tensile tests (static tensile testing) were conducted at room temperature on rectangular proportional specimens with a five-fold gauge length, in compliance with ISO 6892-1:2019. A Zwick-Roell Z100 THW testing machine with a macroXtens® II extensometer was used. The tests were performed under stress-rate-controlled loading. For each sample, the tensile strength (R_m), yield strength ($R_{p0.2}$) and elongation at break (A) were determined. The parameters were calculated as the arithmetic mean of results from at least three specimens for each test point. Additionally, measurement errors were computed as standard deviations based on individual sample results. Impact toughness testing was carried out using a Zwick Roell RPK300 Charpy hammer, with an initial energy value of 300 J, in accordance with ISO 148-1:2017. Rectangular specimens with V-notches were used. Based on test results obtained at a temperature of +20 °C, arithmetic means (from at least three tests per point) and standard deviations of the impact toughness indices were calculated.

Abrasion resistance testing

Abrasion resistance tests were performed using a T-07 tester with loose abrasive material, following the requirements of GOST 23.208-79. A

Table 2. Detailed heat treatment parameters for Hardox Extreme steel

Designation	Heat treatment parameters
HE	As-delivered state (directly after welding)
HE-A(850–1200 °C) Abrasion resistance tests Strength tests	Normalizing: 850 °C, 60 min Austenitization: 850 °C, 900 °C, 1000 °C, 1100 °C, 1200 °C, 120 min, oil
HE, HE-A(850–1200°C) Prior austenite grain size analysis	Normalizing: 850 °C, 60 min Austenitization: 850 °C, 900 °C, 1000 °C, 1100 °C, 1200 °C, 120 min, oil Tempering: 550 °C, 30 min, furnace cooling

constant load of F=44N(ΔF=0.25N) was applied. Test samples measured 30 × 30 × 10 mm. Electrocorundum No. 90 was used as the abrasive material, as per ISO 8486-2:1998. The test duration, depending on material hardness, was set at 1800 roller rotations (30 minutes). Mass loss was measured with a laboratory scale accurate to 0.0001 g. The purpose of the test was to determine the relative abrasion resistance index (k_b) compared to a reference sample made of normalized C45 steel. The abrasion resistance index was calculated using the following Equation 1:

$$k_b = \frac{Z_w \cdot \rho_b \cdot N_b}{Z_b \cdot \rho_w \cdot N_w} \quad (1)$$

where: k_b – relative abrasion resistance index, Z_w – weight loss of reference samples [g], Z_b – weight loss of the tested material [g], N_w – number of roller rotations during reference sample testing, N_b – number of roller rotations during tested sample testing, ρ_w, ρ_b – densities of the reference and tested materials [g/cm^3].

A minimum of five samples were tested for each combination of heat treatment parameters. A schematic of the testing methodology is shown in Figure 2.

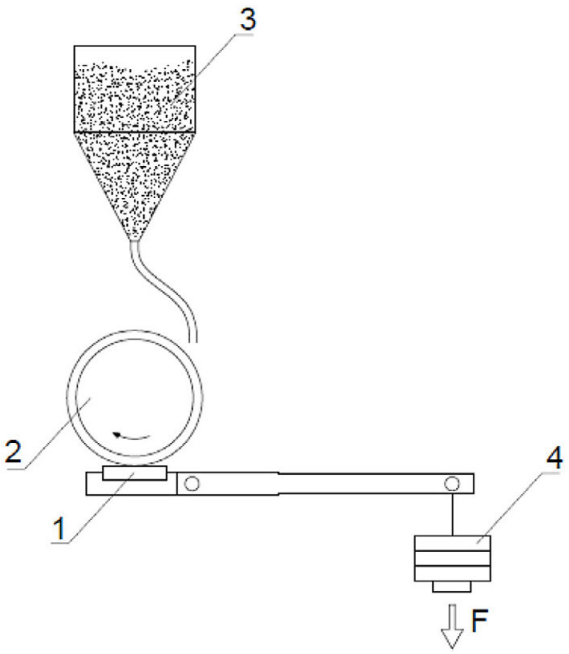

Figure 2. Schematic operation of the T-07 tribotester: 1 – sample, 2 – steel roller with a rubber ring, 3 – abrasive, 4 – load

RESULTS

Microstructural analysis

Based on microscopic images of the Hardox Extreme steel in its as-delivered state, as well as after austenitization in the temperature range of 850–1200 °C, it can be concluded that the microstructure consists of homogeneous martensite (Figures 3a–3f).Laths and needles are observed to undergo more pronounced etching, which may indicate chemical composition microsegregation resulting in carbon-rich microareas or the precipitation of fine-dispersed carbide phases in these regions. This could justify the presence of tempered martensite or lower bainite. To evaluate these areas in detail, scanning electron microscopy (SEM) analysis was conducted. Based on the SEM observations, no fine-dispersed phases providing bright contrast were detected (Figures 4a–4f). Electron microscopy studies confirm the presence of untempered martensite areas and martensite that has undergone coalescence. In the latter case, adjacent martensite blocks sharing the same habit plane and similar crystallographic orientation with respect to the parent austenite tend to overlap and coalesce without the involvement of intermediate phases, forming significantly larger structures. These larger structures are formed during phase transformation by the merging of smaller blocks, each nucleating independently under conditions of prolonged growth. Structures several micrometers in size are surrounded by much smaller blocks. Grain growth is clearly observed with increasing size of packets and blocks in the material quenched within the temperature range of 1000–1200 °C. In these samples, prior austenite grain boundaries are distinctly visible, with some exhibiting a bright network, particularly prominent in samples austenitized at the two highest temperatures (Figures 3e and 3f). Laths and needles grow to substantial sizes, and brighter areas that resist etching are evident between them, indicating a high proportion of retained austenite. Retained austenite grains selectively grow as the austenitization temperature increases, which is also a consequence of chemical composition microsegregation.

An evaluation of prior austenite grain growth (Figure 5) indicates that the applied heat treatment procedures within the 850–900 °C range effectively preserve a fine-grained microstructure. In the as-received condition, the average prior

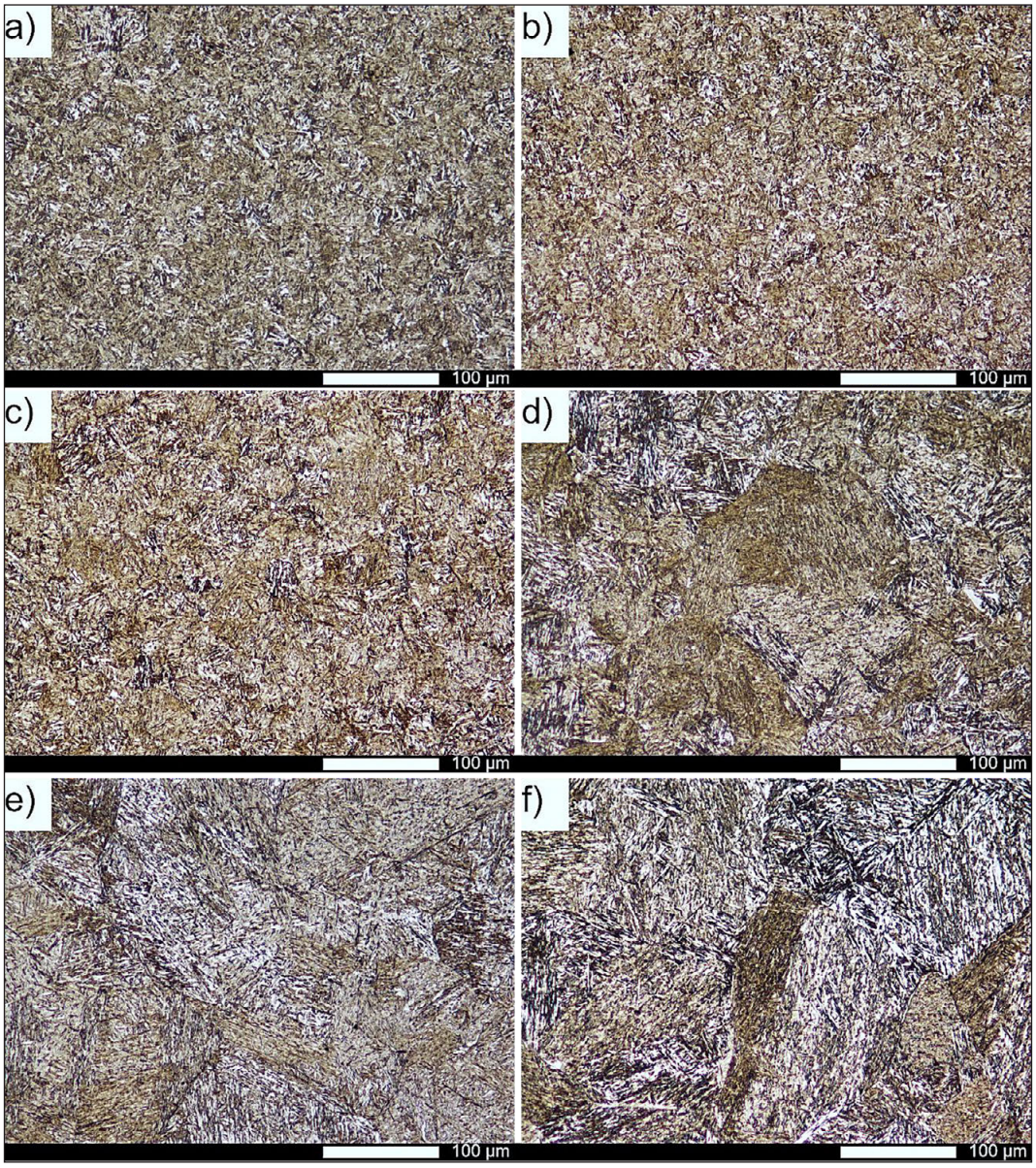

Figure 3. Microstructure of Hardox Extreme steel subjected to heat treatment at different austenitization temperatures: (a) as-delivered state; (b) T_A = 850 °C; (c) T_A = 900 °C; (d) T_A = 1000 °C; (e) T_A = 1100 °C; (f) T_A = 1200 °C. LM, etched with reagent 3 according to ASTM E407

austenite grain size is 16 µm, while austenitization at 850 °C leads to a reduction to 13 µm due to natural microstructure refinement during phase transformation. As the austenitization temperature increases, grain coarsening occurs, reaching 43 µm at 1000 °C and 88 µm at 1100 °C. At the highest investigated temperature of 1200 °C, the grain size expands to 125 µm, with individual grains varying between 25 and 371 µm. The correlation between grain size and austenitization temperature, including the as-delivered state, follows an exponential trend, as illustrated in Figure 5. The visualization of the results also illustrates specific trends. In the as-delivered state and after austenitization at 850 and 900 °C, the average grain size is close to the median, and the difference between the smallest and largest grain sizes is 52 µm, 32 µm, and 28 µm, respectively. Starting from an austenitization temperature of 1000 °C, the median grain size is lower than the average, indicating selective grain growth. The difference between the smallest and largest grain sizes also increases significantly, ranging from 150 µm to 346 µm. This difference is the largest after austenitization at 1200 °C, where the smallest grain size is 25 µm and the largest is 371 µm. Microscopic images and grain size distributions of prior austenite for the as-delivered state and individual

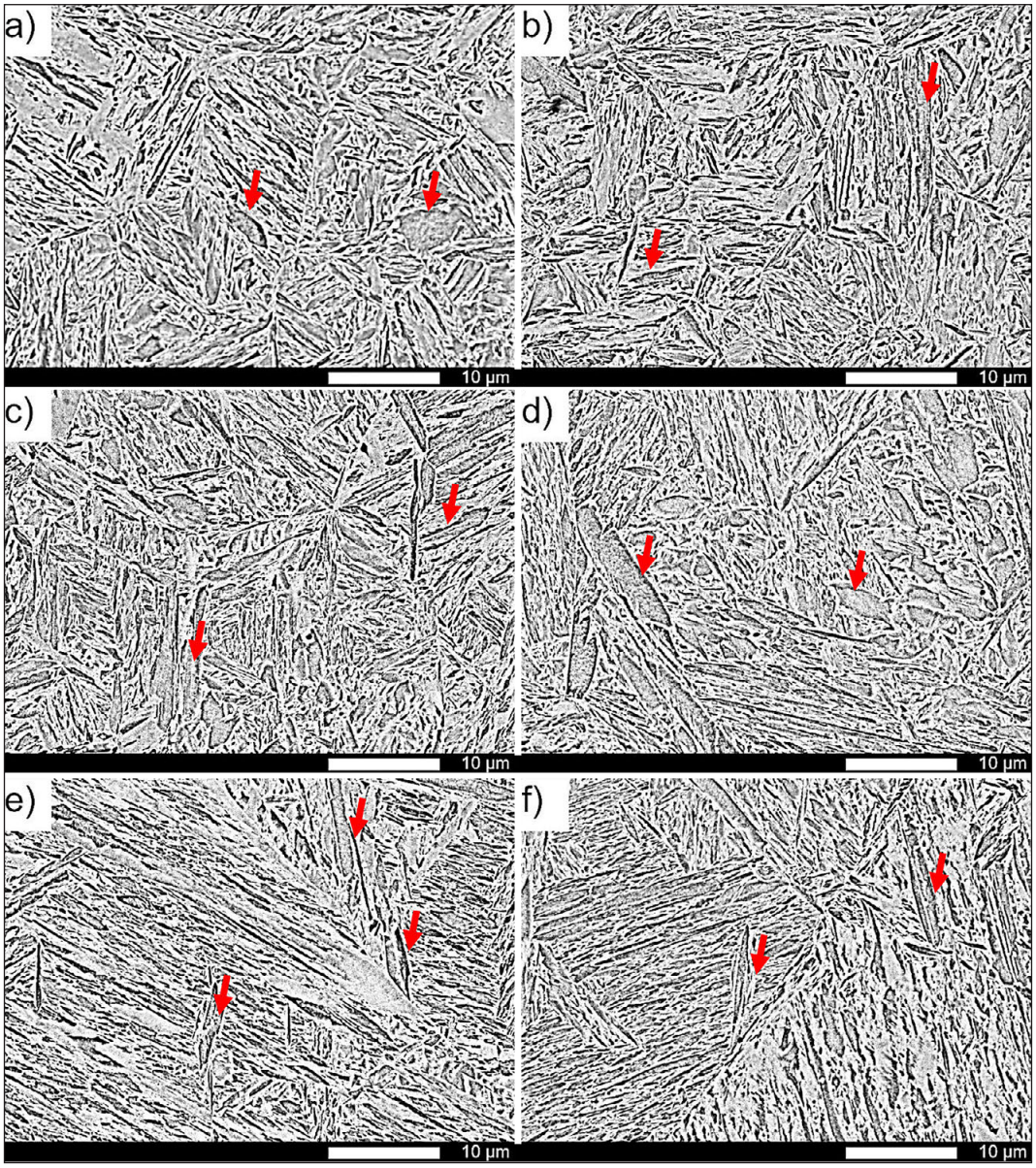

Figure 4. Microstructure of Hardox Extreme steel subjected to heat treatment at different austenitization temperatures: (a) as-delivered state; (b) T_A = 850 °C; (c) T_A = 900 °C; (d) T_A = 1000 °C; (e) T_A = 1100 °C; (f) T_A = 1200 °C. SEM, etched with reagent 3 according to ASTM E407. Arrows indicate martensite undergoing coalescence

austenitization temperatures are shown in Figures 6a–6f and 7a–7f. In the as-delivered state, Hardox Extreme steel exhibits fine grains; however, larger grains can be distinguished, surrounded by colonies of significantly smaller grains (Figure 6a). The microstructure becomes significantly refined, even compared to the as-delivered state, after austenitization at 850 °C, and is characterized by uniform grain size (Figure 6b). This is confirmed by the corresponding grain size distribution, which closely matches a theoretical log-normal distribution (Figure 7b). The most frequent grain size range is 6–14 µm. The minimum and maximum measured grain diameters in this heat treatment condition are 4 µm and 36 µm, respectively. Annealing at 900 °C does not cause significant microstructural changes, resulting in only a slight increase in the parameters characterizing the microstructure (Figure 7c). The morphology remains similar to the microstructure in the as-delivered state (Figure 6c). Differences become apparent only in the grain size distribution (approximated by a log-normal distribution), which indicates that the largest share of the microstructure consists of grains sized 12–16 µm. More pronounced changes occur after heat treatment at 1000 °C (Figure 6d), where the recorded grain sizes range from 10 µm to 160 µm (Figure 7d). These differences in

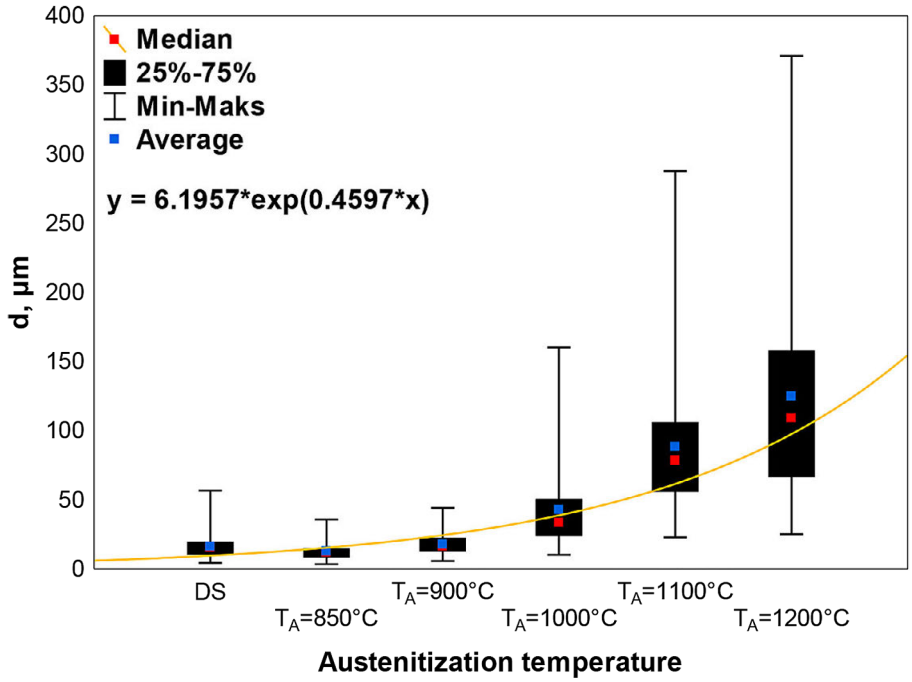

Figure 5. Descriptive statistics of grain size distributions in Hardox Extreme steel for different austenitization temperatures

grain size are due to the abnormal growth of some grains. This process becomes more intense during austenitization at 1000 °C, leading to a clear division of microstructural components into abnormal grains and surrounding colonies of smaller grains, which also gradually grow. Abnormal grains reach relatively large sizes, preventing the microstructure from being considered fine-grained. These processes advance significantly during austenitization at 1100 °C (Figures 6e and 7e), where noticeable grain growth results in a coarse-grained microstructure. Colonies of smaller grains are no longer observed, except for a few isolated smaller grains. This trend continues after annealing at the highest temperature, where the most frequent grain size range is 54–83 µm (Figures 6f and 7f). It should be noted that all empirical distributions of austenite grain size can be approximated by a log-normal distribution. Preliminary conclusions regarding changes in the martensitic microstructure morphology have been confirmed, namely, grain growth in Hardox Extreme steel occurs rapidly. For heat treatment planning, a temperature of 950 °C can be considered safe. This behavior is due to the chemical composition of Hardox Extreme steel, which lacks alloying elements that form stable carbides. Thus, grain boundary migration can only be effectively impeded by aluminum nitride precipitates.

Mechanical properties

Figures 8–11 present the results of hardness measurements, static tensile tests, and impact toughness tests. The hardness of Hardox Extreme steel in the as-delivered state is lower than the value declared by the manufacturer, measuring 583 HBW. After austenitization at the lowest temperature, the hardness increases to 611 HBW, approximately 5% higher than in the as-delivered state. A further increase in hardness, about 7% compared to the as-delivered state, is observed after annealing at 900 °C. Consequently, the highest hardness value of the steel is achieved under this heat treatment condition. Increasing the austenitization temperature leads to a gradual reduction in hardness. However, the obtained values remain higher than in the as-delivered state, even after heat treatment at the highest temperature. It is noteworthy that after austenitization at 1100 °C, the hardness reaches levels comparable to those observed after heat treatment at 850 °C. Referring solely to the heat-treated states examined in this manuscript, the difference in hardness between the extreme values is 37 HBW, which represents just over 6% relative to the state with the lowest hardness. This indicates that hardness, in the case of Hardox Extreme steel, does not exhibit significant sensitivity to changes in PAGS.

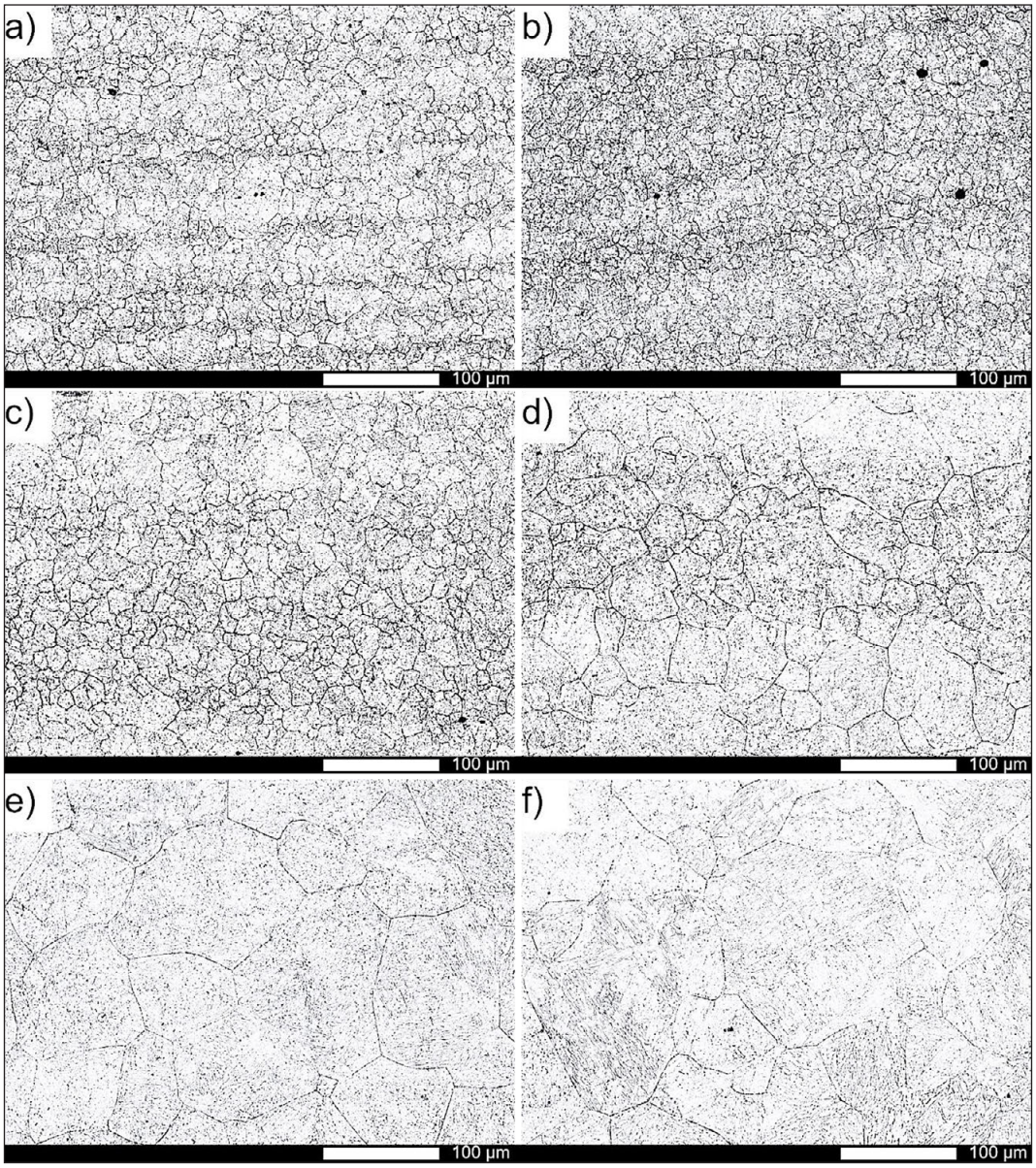

Figure 6. Microstructures of Hardox Extreme steel with revealed prior austenite grain boundaries: (a) as-delivered state; (b) T_A = 850 °C; (c) T_A = 900 °C; (d) T_A = 1000 °C; (e) T_A = 1100 °C; (f) T_A = 1200 °C. LM, etched with reagent 79 according to ASTM E407

The tensile test results are presented in Figures 9 and 10. These results indicate that in the as-delivered state, Hardox Extreme exhibits high strength properties but unsatisfactory plasticity characteristics. The tensile strength (R_m) and yield strength ($R_{p0.2}$) are 2123 MPa and 1630 MPa, respectively. The elongation at break (A) slightly exceeds 9%. After austenitization at 850 °C, the strength indices decrease. The tensile strength is 2112 MPa (a reduction of 0.5% compared to the as-delivered state), while the yield strength drops to 1521 MPa (a reduction of nearly 7% compared to the as-delivered state). Notably, the reduction in yield strength is more pronounced. This observation justifies the calculation of the ratio of yield strength to tensile strength for the analyzed heat treatment conditions. In this heat-treated state, the ratio is 0.72, compared to 0.77 in the as-delivered state. The material also exhibits satisfactory ductility, represented by an elongation at break of A = 9.4%. In the state quenched from 900 °C, the material shows excellent strength parameters. There is an increase in tensile strength (R_m = 2176 MPa) and yield strength ($R_{p0.2}$ = 1561 MPa) compared to the state quenched from the lower temperature, with a relative increase of approximately 3%. Consequently, the $R_{p0.2}/R_m$ ratio is 0.71. However, there is a slight reduction in

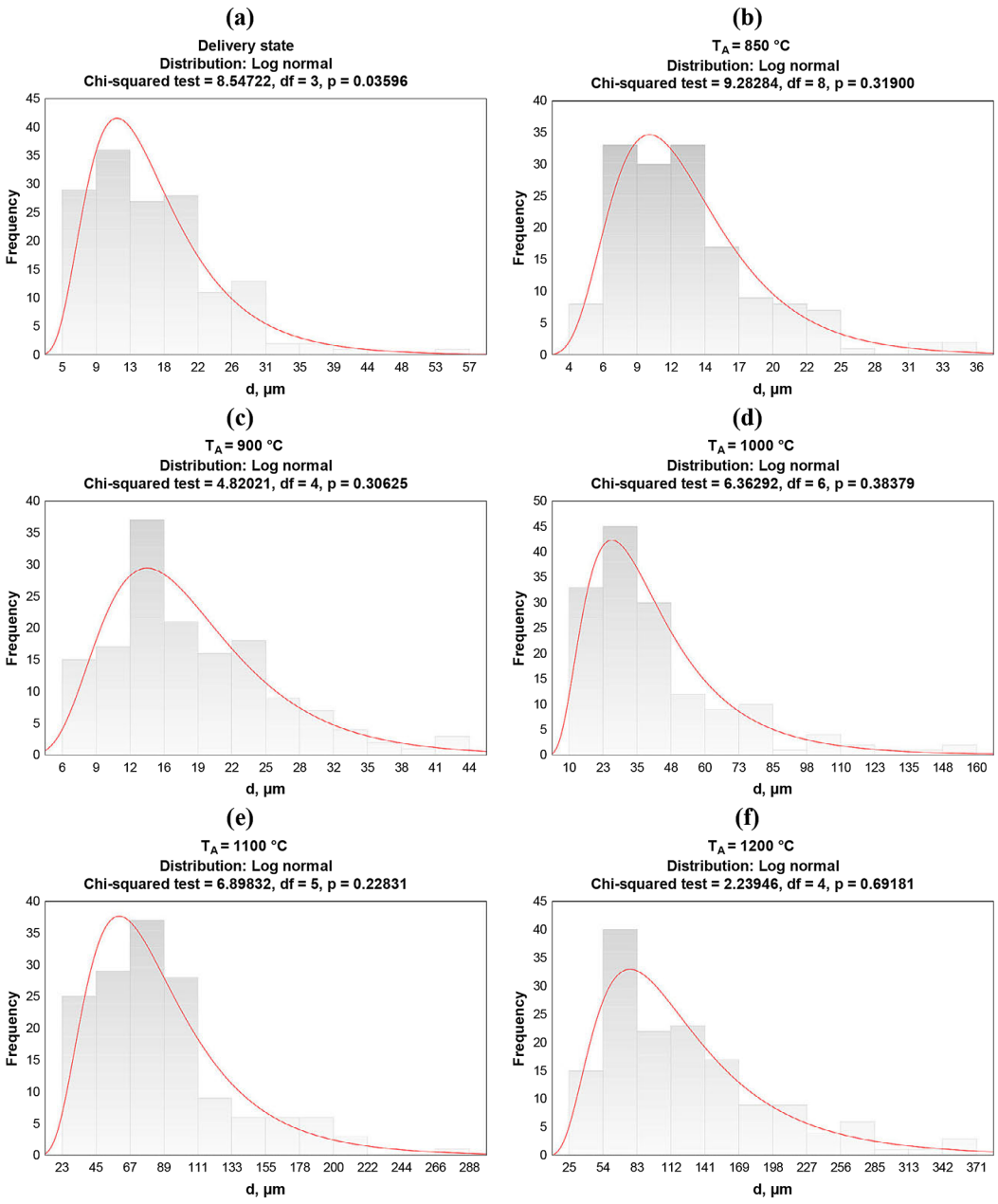

Figure 7. Grain diameter distributions for austenite in Hardox Extreme steel:
(a) as-delivered state; (b) T_A = 850 °C; (c) T_A = 900 °C; (d) T_A = 1000 °C; (e) T_A = 1100 °C; (f) T_A = 1200 °C

ductility, with the elongation at break decreasing to A = 8.8%. High strength properties – 2130 MPa and 1548 MPa ($R_{p0.2}/R_m$ = 0.73) are maintained after heat treatment involving austenitization at 1000 °C. However, these properties are not accompanied by satisfactory plasticity, as indicated by the elongation at break (A = 6.2%), the lowest value among all heat-treated states. After quenching from 1100 °C, the strength indices decrease compared to the state heat-treated at a lower temperature, with values of R_m = 2118 MPa and $R_{p0.2}$ = 1455 MPa. In this heat-treated state, the elongation at break is A = 7.5%. The reduction in strength parameters continues with increasing austenitization temperature. For the state heat-treated at the highest temperature, the tensile strength of Hardox Extreme steel is R_m = 2023MPa, and the yield strength is 1440 MPa ($R_{p0.2}/R_m$ = 0.71), representing a reduction of over 7% compared to the heat-treated states examined in this study. However, it is worth noting that in all heat-treated states, the tensile strength exceeds 2000 MPa. Simultaneously, as the austenitization temperature increases, the elongation at break decreases to A = 6.5%. The observations outlined above lead to the conclusion that increasing the

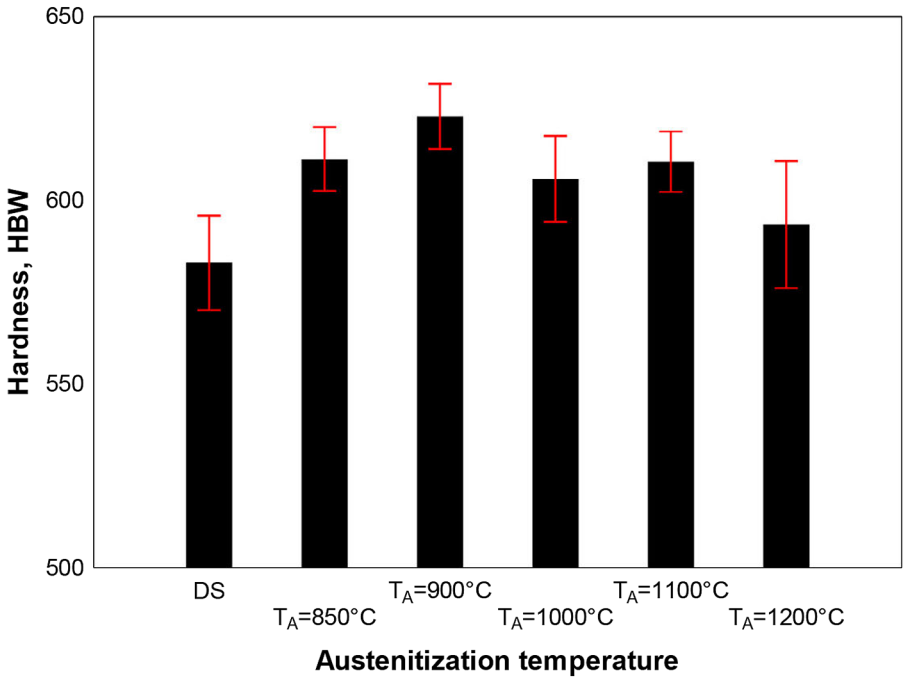

Figure 8. Hardness of Hardox Extreme steel in the as-delivered state and at various austenitization temperatures (DS – delivery state)

austenitization temperature beyond 1000 °C, and consequently increasing the PAGS, results in a reduction of both strength and ductility indices under static loading conditions.

Impact testing of Hardox Extreme steel revealed that its resistance to dynamic loads remains below 35 J/cm^2, which defines the lower threshold for material brittleness [10] (Figure 11). In the as-delivered state, the impact toughness is approximately 17 J/cm^2. Heat treatment at various quenching temperatures increases this value, reaching a maximum of approximately

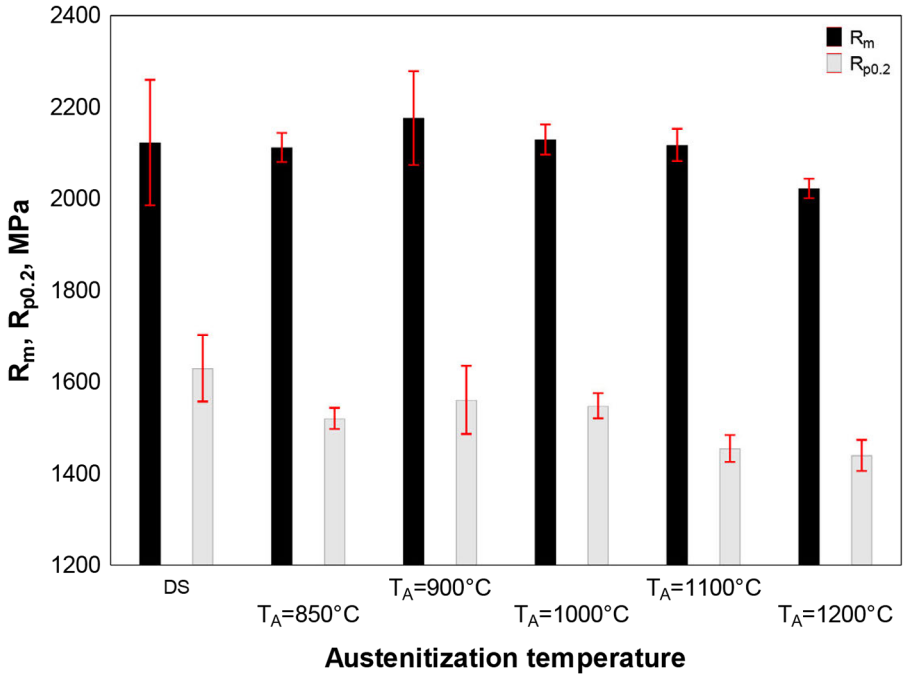

Figure 9. Tensile strength and yield strength of Hardox Extreme steel in the as-delivered state and at various austenitization temperatures (DS – delivery state)

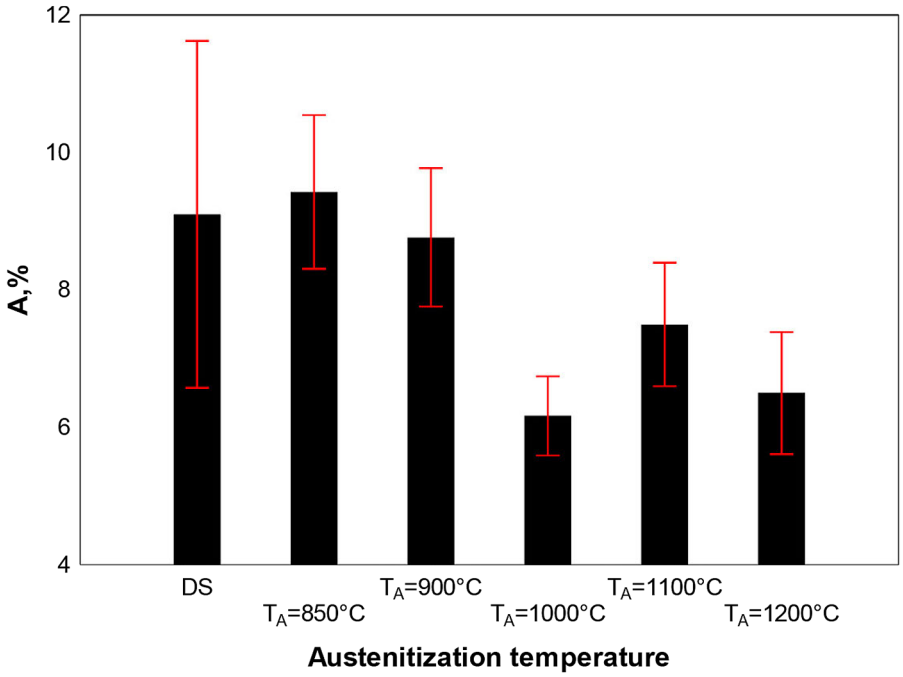

Figure 10. Elongation at break (A) of Hardox Extreme steel in the as-delivered state and at various austenitization temperatures (DS – delivery state)

33 J/cm^2 for material austenitized at 850 °C and 900 °C. Increasing the austenitization temperature reduces the impact toughness to 22 J/cm^2 (T_A = 1100 °C); however, after quenching from 1200 °C, the impact toughness rises to 29 J/cm^2. It should be noted that in all cases, the obtained values indicate low ductility and limited operational potential of the steel. Comparing the results, it is evident that impact toughness decreases by over 33% between the mean values for austenitization temperatures of 850 °C and 1100 °C. This confirms the trend observed in the tensile

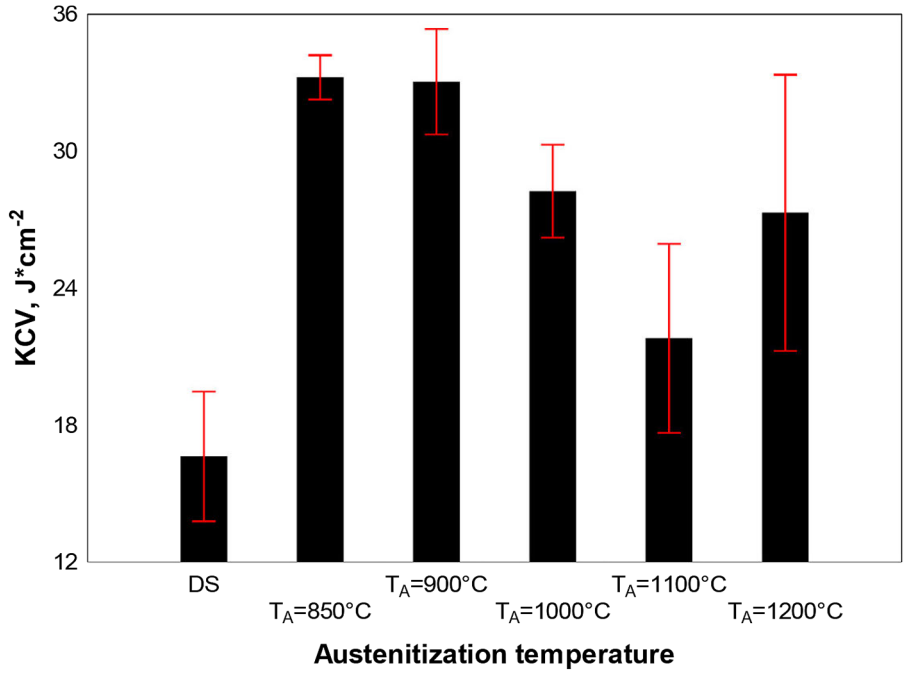

Figure 11. Impact toughness (*KCV*) of Hardox Extreme steel in the as-delivered state and at various austenitization temperatures (DS – delivery state)

tests, unequivocally demonstrating a decline in the material's plasticity properties as the austenitization temperature exceeds 900 °C (Figure 10). Another noteworthy observation is the very low impact toughness in the as-delivered state, which features a grain size comparable to the state austenitized at 900 °C. The relative change in austenite grain size between the as-delivered state and the state after austenitization at 900 °C is approximately 12%. However, the impact toughness increases by 94%. Furthermore, for the state heat-treated at the highest temperature, a 23% increase in impact toughness is recorded compared to the state austenitized at 1100 °C. This could be attributed to the significant presence of retained austenite in the microstructure. Overall, the results demonstrate that, despite relatively low values, impact toughness is dependent on the austenite grain size. Therefore, the fracture characteristics should also be assessed through both macroscopic and microscopic analysis.

The fractographic analysis revealed similar features, allowing the fracture surfaces of the samples to be divided into two groups (Figure 12). The first group includes fractures of the steel in the as-delivered state and after austenitization at 850 °C and 900 °C. These fractures exhibit a matte, fine-grained surface. No plastic deformation is observed, and the surface appears smooth, with occasional steps and lateral fracture zones, representing ductile fractures. The overall share of these zones in the entire fracture is between 15% and 20%. Practically no plastic zones were observed directly below the mechanical notch or at edges opposite the notch, except for the fracture of the steel in the as-delivered state. The second group consists of fractures of samples austenitized in the temperature range of 1000–1200 °C. Based on macroscopic images, it can be concluded that these fractures feature larger contributions of plastic zones in the lateral areas and opposite the mechanical notch. The proportion of plastic zones in the samples is 29%, 22%, and 25% for austenitization at 1000 °C, 1100 °C, and 1200 °C, respectively. The surfaces exhibit distinct roughness and reflect the grain size, showing features typical of this type of decohesion. This suggests that the steel austenitized at the highest temperatures is characterized by a distinctly coarse-grained structure. Additionally, no macroscopic signs of plastic deformation were observed in the fractures of any of the samples.

Microscopic examinations revealed that in all cases, the fracture surfaces exhibit features characteristic of quasi-cleavage fractures. Therefore,

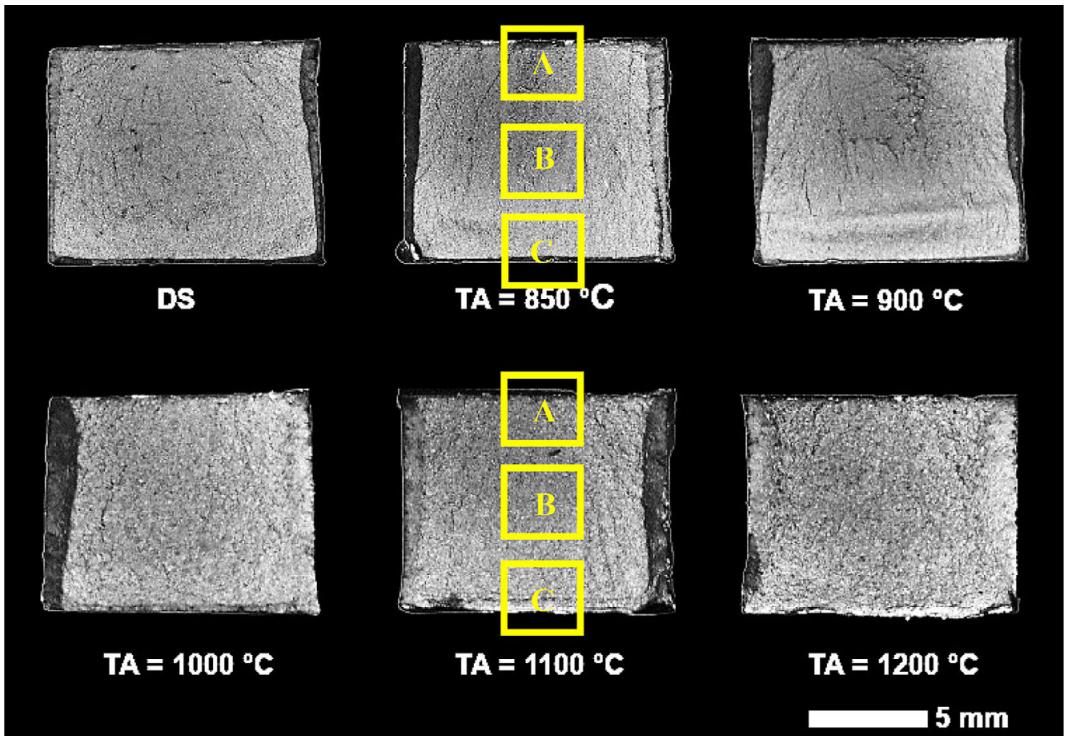

Figure 12. Macroscopic images of fracture surfaces in Hardox Extreme steel in the as-delivered state and after austenitization at different temperatures. A, B, and C – locations of microscopic analyses

detailed fractographic documentation of characteristic zones (zone under the notch A, central zone B, and lateral fracture zone C) is provided only for the as-delivered state (Figures 13a–13c), after austenitization at 850 °C (highest impact toughness) (Figures 13d–13f), and after austenitization at 1100 °C (lowest impact toughness) (Figures 13g–13i).

The selected fracture zones of Hardox Extreme steel, shown in Figures 13a–13i for different heat treatment conditions and tested at room temperature, exhibit significant morphological similarities when considering the influence of austenitization temperature. The slight differences noted in quantitative analyses mainly stem from variations in the proportion of plastic zones observed in the macroscopic images. The microstructure analysis of individual zones revealed the presence of mixed fractures. The dominant feature is a quasi-cleavage fracture interspersed with small plastic zones. Quasi-cleavage fractures are primarily characteristic of heat-treated steels or those fractured below the brittle temperature threshold. They form through the coalescence of local cracks that may lie on the same plane. The expansion of voids leads to significant plastic deformation before they merge, ultimately resulting in tearing along sharp edges, referred to as separations or ridges [37]. This distinctive structure originates from micropores or microcracks that grow until they join. The fracture behavior depends on the size of martensite plates, and therefore the elementary fracture surfaces are also influenced by the PAGS [37]. It was found that in polycrystalline materials, some grains have orientations or stress states unfavorable for cleavage fracture, which manifests as plastic fracture zones. This type of structure is typically observed in fracture zones with a clearly refined microstructure. Such topographic fracture structures were observed in the as-delivered state and after austenitization at 850 °C (Figures 13a–13f). Conversely, the dimple structure observed on the fracture surfaces is mainly characterized by a regular but parabolic outline and high refinement, indicating crack initiation through plastic deformation. This shape results from slip and decohesion of the crystallographic structure, evident as overlapping scales along the {100} planes [38]. Within the dimples, isolated phase precipitates related to the chemical composition were observed. Since most exposed surfaces exhibited characteristic "river" morphology, precise identification of these planes was practically impossible. This can be attributed to the formation of a widespread dimple structure, typical of ductile fracture, caused by the "meandering" of the aforementioned river system. It is worth mentioning that increased energy absorption during fracture, and thus a reduction in the brittleness threshold, is often associated with the formation of mixed fractures, referred to as steps. In the zones under the mechanical notch and opposite the mechanical notch, no typical plastic zones were observed (Figures 13a, 13c, 13d, and 13f). However, approaching the edges, the proportion of plastic bands consisting of small dimples increases. These dimples contained phase precipitates and non-metallic inclusions.

For the sample austenitized at 1100 °C, the individual zones are also similar to one another and consist of a transgranular mixed fracture, with quasi-cleavage and ductile characteristics, exhibiting significant irregularity of the fracture plane (Figures 13g–13i). Transverse cracks, along with characteristic oval indentations and separations, were also observed. The area located on the side opposite the mechanical notch represents a typical ductile fracture with parabolic-shaped dimples, referred to as a shear-formed "scaly" fracture (Figure 13i). This structure comprises a system of oval elevations and depressions formed as a result of plastic deformation. Transverse cracks running partially along grain boundaries are also visible. Although the surface retains a complex topography, there is a noticeable reduction in the extent of plastic zones and a less developed system of plastically deformed "rivers" and separations located on the edges of quasi-cleavage facets, characteristic of this type of fracture. The fracture surface is characterized by a pronounced topography with larger elevations and depressions. Furthermore, numerous transverse cracks and a significant proportion of typically cleavage areas with internal grain separations are evident. The presence of these areas significantly reduces impact toughness compared to samples austenitized at lower temperatures. Cracks continue to form branches but less intensively than in samples austenitized at lower temperatures, likely influenced by the increased grain size of the tested steel. It is assumed that secondary cracks propagate in the immediate vicinity of the main crack, as long as they exhibit characteristic discontinuities (the crack is formed by a system of fine microcracks). One of

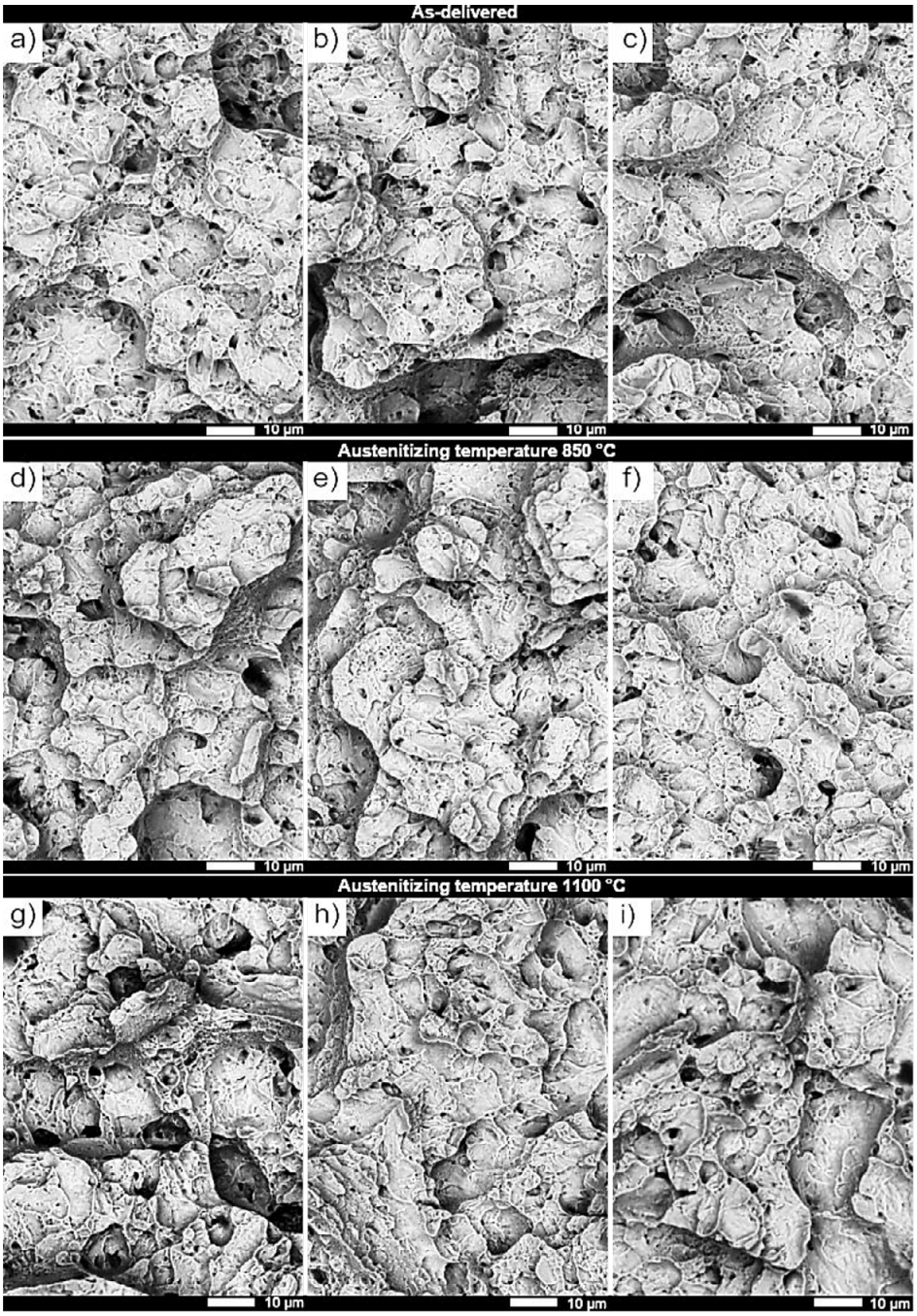

Figure 13. Fracture surface images of Hardox Extreme steel after impact testing at +20 °C: (a) as-delivered state, zone under the mechanical notch, (b) as-delivered state, central zone, (c) as-delivered state, zone opposite the mechanical notch, (d) T_A = 850 °C, zone under the mechanical notch, (e) T_A = 850 °C, central zone, (f) T_A = 850 °C, zone opposite the mechanical notch, (g) T_A = 1100 °C, zone under the mechanical notch, (h) T_A = 1100 °C, central zone, (i) T_A = 1100 °C, zone opposite the mechanical notch. SEM, non-etched state

the causes of these microcracks is the formation of microsteps on the fracture surface, attributable to internal structural defects. Qualitative changes observed in this fracture, compared to the previously discussed fractures, include an increase in the size of dimples, elevations, and depressions, which appear to reflect the prior austenite grain structure. Additionally, in quasi-cleavage zones, the presence of rivers and tributaries is reduced, indicating lower energy expenditure in their formation. Therefore, the reduction in impact toughness at the analyzed austenitization temperature is more influenced by the smaller proportion of plastic zones under the mechanical notch and at the edges, rather than the proportion of these zones in the central part of the fracture.

Abrasion resistance

The results of the abrasion resistance tests revealed that increasing the austenitization temperature leads to a decrease in abrasion resistance by approximately 4% (Figure 14). Notably, austenitization at the lowest tested temperature of 850 °C enhances abrasion resistance, as evidenced by an increase in the relative wear resistance coefficient. In the as-received condition, the k_b value is 1.34, whereas after heat treatment at 850 °C, it rises to 1.37. The material austenitized in temperatures between 900 °C and 1100 °C exhibits comparable values (k_b = 1.35). The lowest value is recorded for the material quenched from the highest austenitization temperature (k_b = 1.32). However, the obtained coefficients remain satisfactory and demonstrate that the PAGS has a limited quantitative effect on abrasion resistance in the presence of loose abrasive material. The surface images of samples subjected to abrasion tests (Figures 15a–15i) show that grain growth negatively impacts abrasion resistance, considering the observed and defined wear micromechanisms. The least intense changes are observed in the material quenched from 850 °C (Figures 15d–15f). The scratches visible on the sample surfaces are narrow, aligned with the direction of abrasive movement, and exhibit only a few indentations caused by embedded abrasive grains. The primary wear mechanism is micro-cutting, although traces of plastic deformation are also observed. The surface of the material in the as-delivered state features irregularly distributed indentations, with ridges of deformed material forming at their intersections (Figures 15a–15c). Fragments resulting from the generation of low stresses also significantly contribute to the wear process, with micro-cutting and chipping being the primary material removal mechanisms. As the heat treatment temperature increases, the abrasive grains' penetrating interaction intensifies (Figures 15g–15i). In all cases, progressively wider scratches, deep and broad pits, and plastically deformed material raised above the surface are observed. This material does not detach quickly under the cyclic action of abrasive particles, which results in mass losses comparable to those of other samples, as measured after the abrasion test, leading to similar k_b values. The scratches are increasingly extensive compared to materials quenched at lower temperatures, and the surface condition is the most defected. Between the scratches and grooves, smoothed areas are visible, indicating an ongoing mechanism of irregularity cutting.

The above observations also apply to microstructural changes in the subsurface zones subjected to abrasion tests (Figures 16a–16f). In none of the observed cases is there evidence of deformation in the martensitic microstructure, meaning that martensite blocks do not plastically yield under the action of abrasive grains. The edges are

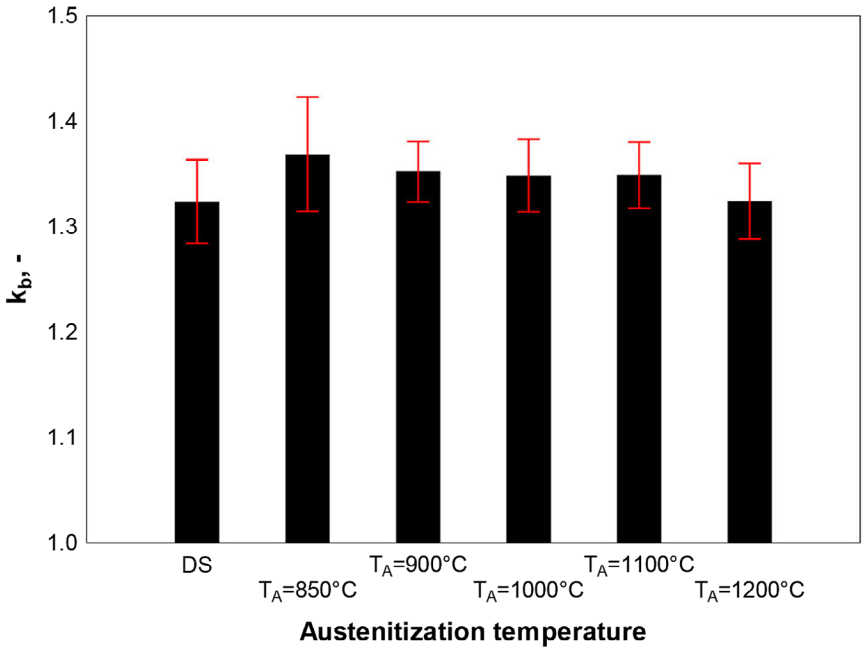

Figure 14. Relative abrasion resistance coefficient k_b of Hardox Extreme steel at various austenitization temperatures (DS – delivery state)

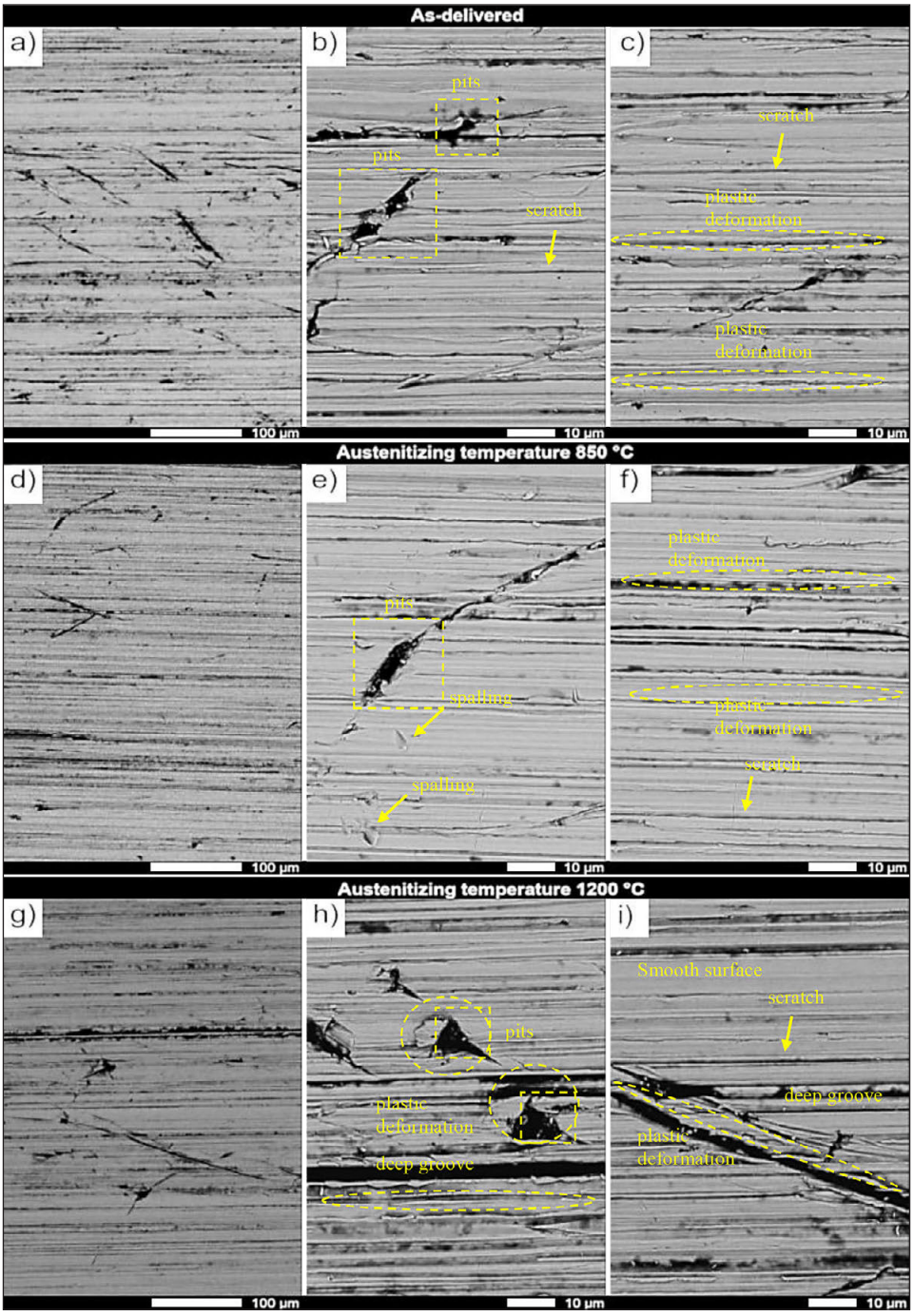

Figure 15. Surface images of Hardox Extreme steel samples subjected to abrasion tests: (a) as-delivered state, magnification 1000x, (b) as-delivered state, magnification 5000x, (c) as-delivered state, magnification 5000x, (d) T_A = 850 °C, magnification 1000x, (e) T_A = 850 °C, magnification 5000x, (f) T_A = 850 °C, magnification 5000x, (g) T_A = 1200 °C, magnification 1000x, (h) T_A = 1200 °C, magnification 5000x, (i) T_A = 1200 °C, magnification 5000x. SEM, non-etched state

sharp or smoothed, and grooves can be observed locally. However, the width and depth of the resulting scratches increase with higher austenitization temperatures. Based on the observed micromechanisms of abrasive wear, a certain regularity can be noted: larger austenite grains result in deeper and wider scratches and grooves.

DISCUSSION

The study also attempted to correlate the PAGS with hardness, tensile strength, yield strength, elongation at break, impact toughness, and abrasion resistance measured by the k_b coefficient. The results of this analysis are shown in

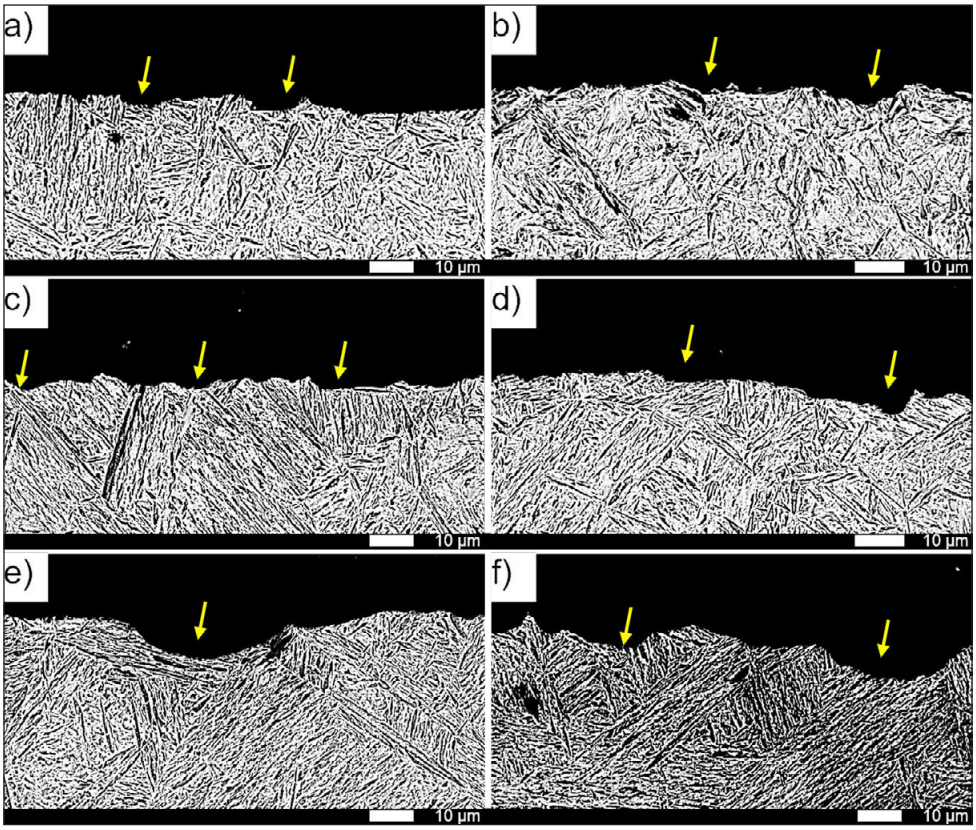

Figure 16. Microstructure of cross-sections of samples subjected to abrasion tests, transverse to the abrasive movement direction: (a) as-delivered state; (b) T_A = 850 °C; (c) T_A = 900 °C; (d) T_A = 1000 °C; (e) T_A = 1100 °C; (f) T_A = 1200 °C. SEM, etched with reagent 3 according to ASTM E407. Arrows indicate examples of pits and grooves. SEM, non-etched state

Figures 17a–17f. In each case, the obtained results were approximated using a second-degree polynomial. However, when considering the parameters analyzed for the as-delivered state relative to the grain size in this heat treatment condition, the determination coefficient of the resulting function did not indicate sufficient model fit. As the parameters of the specific heat treatment and mechanical processing of Hardox Extreme steel are proprietary to the manufacturer, the authors decided to perform a similar approximation of the results while excluding the as-delivered state. As a result, in each case, the best model fit was achieved using a second-degree polynomial, with the determination coefficient ranging from 0.6173 to 0.9420. Approximating the results with a second-degree polynomial also indicates the existence of an optimal grain size at which the evaluated parameters reach a minimum or maximum value. The variation in mechanical properties depending on grain size is indeed influenced by different features reflected in martensite morphology. In the same area, smaller grains contain more blocks and packets, which are associated with higher dislocation density [16]. For hardness, the overall trend of the results aligns with that of Hardox 450 steel [26]. In the case of Hardox 450 steel, the lowest hardness value, 464 HV1, is observed in the as-delivered state (similarly to Hardox Extreme steel), whereas the highest hardness is found in the steel austenitized at 950 °C, reaching a hardness of 536 HV1 (comparable to Hardox Extreme steel austenitized at 900 °C). Thus, as with Hardox 450 steel, no correlation was observed between the hardness of the analyzed material grade and its grain size (determination coefficient 0.6477, excluding the as-delivered state) (Fig. 17a). A study conducted by Li et al. [39], found that microstructure refinement has little impact on strength properties such as hardness. However, the authors explain this as follows: larger austenite grains lead to a higher martensitic transformation temperature, which can result in stronger solid-solution strengthening and, consequently, an increase in dislocation density. For tensile strength, the obtained results were approximated with quadratic functions, whose determination coefficients were similar

regardless of whether the as-delivered state was included (Figure 17b). Moreover, the determination coefficients, 0.8033 and 0.8151, indicate a high consistency between the models and the experimental data. As the average PAGS increases, tensile strength reaches a maximum value, after which a decline is observed. This relationship suggests that grain size influences the fracture mechanism. Literature data [40, 41] confirm that this dependency is particularly evident in bainitic and martensitic steels, where austenite grain refinement not only increases strength but also improves ductility. The significantly higher number of high-angle grain boundaries (>45°) resulting from smaller grains supports strain energy accumulation and reduces the risk of fracture. This is because the PAGS in bainitic and martensitic steels is also associated with an increase in block and packet sizes, which negatively affects the strength and ductility of the steel [40, 41].

Significant differences between the determination coefficients were observed for the yield strength (Figure 17c). The determination coefficient for data including the as-delivered state was 0.7102, while for data excluding this state, it reached 0.8164. In both cases, a decrease in yield strength was evident with increasing grain size, consistent with the Hall-Petch relationship. The Hall-Petch relationship primarily applies to materials with a body-centered cubic (BCC) crystalline structure. Moreover, for high-strength steels, the *ky* values vary between 450 and 2190 MPa·μm$^{-1/2}$, depending on the structural level controlling strength properties (e.g., lath size, block size, or PAGS) [41]. Transforming the experimental results to derive the Hall-Petch relationship for the analyzed steel (Figure 18), it was found that the k_y value for Hardox Extreme steel was 1607 MPa·μm$^{-1/2}$ (excluding the as-delivered state), consistent with previous observations [41]. The high correlation coefficient between the experimental data and the regression curve confirms that changes in yield strength in Hardox Extreme steel occur linearly and depend on the inverse square root of the PAGS. This phenomenon is supported by numerous studies, for example, on Hardox 450 [23], CrMoV [42], czy 0.1C-5Mn [29], including austenitic steels. Additionally, with decreasing strength indices, a reduction in elongation at break is also observed [23, 29], consistent with the findings for Hardox Extreme steel (Figure 17d). However, it should be noted that for this parameter, determination coefficients of 0.6770 and 0.6173 indicate a general trend of reduced ductility with increasing grain size. In this context, it is necessary to consider a stricter criterion of ductility, such as impact toughness.

Numerous studies have evaluated the impact of austenite grain size on impact toughness. While microstructure refinement has shown a limited effect on strength indicators, it significantly influences impact toughness. For Hardox Extreme steel (Figure 17e), the results indicate a notable reduction in impact toughness only after austenitization at 1100 °C, corresponding to an average grain size of 88 μm. Therefore, impact toughness shows only a slight decline as the austenite grain size increases from 16 to 43 μm, which aligns with observations by Wang et al. [43], who noted a minimal reduction in impact toughness for 22MnB5 steel with grain sizes ranging from 18 to 38 μm. Examining the impact toughness of martensitic steels with increased wear resistance reveals a strong dependence on grain size in lower-grade steels such as Hardox 450 [23]. The change in austenite grain size in Hardox 450 significantly affects impact toughness, reducing the proportion of plastic zones at the fracture edge and altering the character of the central quasi-cleavage zone. In the latter, the proportion of plastic ridges decreases, typical brittle facets emerge, and the propagation mode of secondary cracks changes. Furthermore, the first significant reduction in impact toughness occurs when the austenite grain size increases from 18 to 35 μm. This initial phase of grain growth is critical in the context of reduced ductility. However, impact toughness values below the critical threshold of 35 J/cm² were not reached until the grain size grew to approximately 90 μm. The safety margin in impact toughness stems from the high initial toughness of the steel. For Hardox Extreme steel, the anomalous increase in impact toughness observed after austenitization at the highest temperature is intriguing. This can be attributed to the significant presence of retained austenite in the microstructure, which supports a level of ductility. According to Chen et al. [44] retained austenite significantly influences impact toughness, even at cryogenic temperatures. When considering abrasion resistance, the effect of retained austenite on this parameter is inconclusive, with conflicting results reported [45]. Some research teams report a positive effect of retained austenite due to its work-hardening capability, which may apply to impact-abrasion wear. However, other studies suggest either a negative impact or

no effect of retained austenite on tribological resistance. For the abrasion resistance considered, no significant quantitative effect of PAGS was observed (Fig. 17f). However, notable changes occurred in the wear micromechanisms, reflected in the quality of the resulting surfaces. Nevertheless, a general trend can be established: as grain size increases, abrasion resistance decreases. The observed changes could have implications in impact-abrasion testing (high-stress abrasive tests), as demonstrated with a commercial abrasion-resistant steel with a hardness of 500 HB [18]. The highest abrasion resistance was observed in material with the smallest and most uniform austenite grains. For lower-grade steels [26] the lowest abrasion resistance coefficient was recorded for steel austenitized at 1100 °C, while the highest was for a sample austenitized at 900 °C. In the case of Hardox 450 steel, changes in the austenite grain size in the microstructure influenced the average weight loss rate during wear, with particularly noticeable increases in wear occurring in the presence of abnormal grains. Grains smaller than 40 µm demonstrated higher abrasion resistance than grains considered abnormal in size. A similar correlation between weight loss and grain size was reported in [27, 32]. However, despite achieving a determination coefficient of 0.7814, indicating a good model fit, the differences in weight loss between individual samples were small enough to

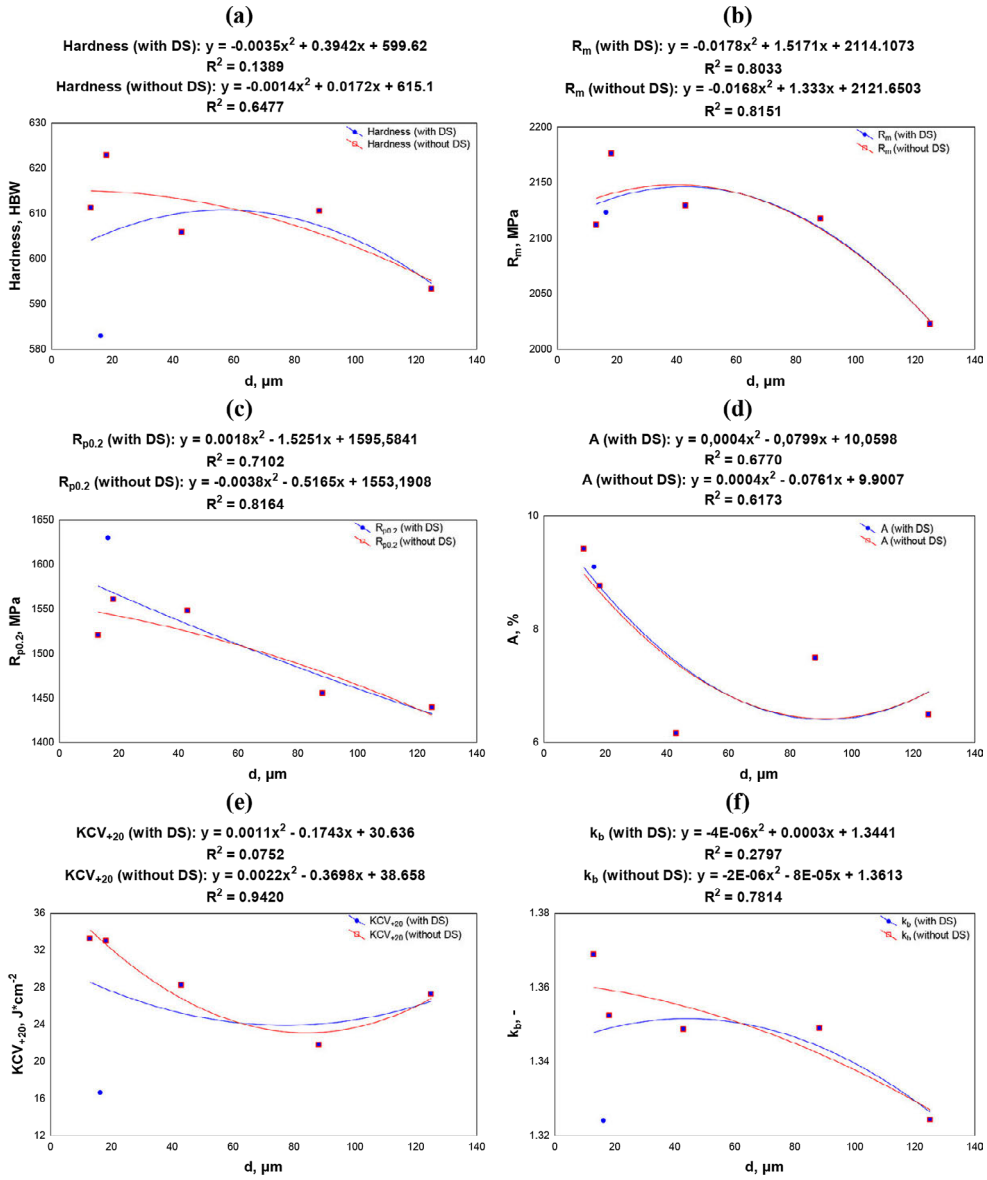

Figure 17. The effect of PAGS on selected mechanical properties of Hardox Extreme steel: (a) hardness, (b) tensile strength, (c) yield strength, (d) elongation at break, (e) impact toughness, (f) abrasion resistance. DS – delivery state

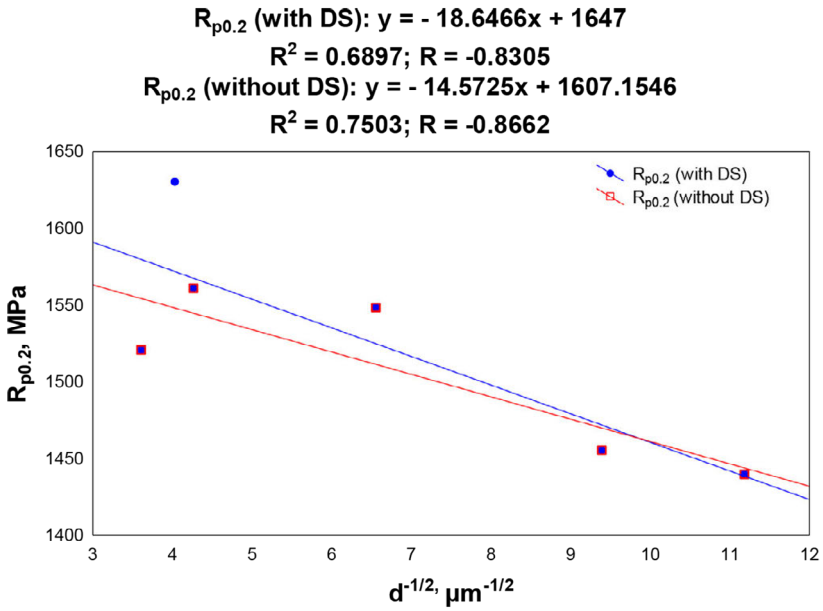

Figure 18. The effect of the inverse square of PAGS on yield strength. DS – delivery state

make it difficult to clearly identify the influence of PAGS on abrasion resistance in high-strength Hardox Extreme steel. Numerous studies indicate that the PAGS can indirectly affect tribological resistance [32]. Experimental evidence has shown that reducing PAGS decreases the size of packets and blocks. Consequently, the combination of strength, ductility, and impact toughness significantly increases as packet/block size decreases.

CONCLUSIONS

This study compiles the results of research on Hardox Extreme steel, a low-alloy boron steel with enhanced resistance to abrasive wear. The objective was to determine the effect of PAGS on its mechanical properties, with particular emphasis on abrasion resistance. The objective was achieved through the following tasks. Increasing the quenching temperature results in a uniform martensitic microstructure, with features such as laths and needles that are more susceptible to etching, potentially indicating microsegregation of chemical composition and the formation of microareas richer in carbon. After austenitization at 1100 °C and 1200 °C, the laths and needles grow larger, and visibly lighter areas appear between them, which are not affected by etching, suggesting a significant presence of retained austenite. Grains containing retained austenite selectively grow as the austenitization temperature increases. The hardness, tensile properties, elongation at break, impact toughness, and fracture behavior of Hardox Extreme steel vary significantly depending on the heat treatment state. The lowest hardness value (583 HBW) was observed in the as-delivered state, while the highest (623 HBW) was recorded after austenitization at 900 °C. The as-delivered state exhibited some of the highest tensile properties (Rm = 2123 MPa, Rp0.2 = 1630 MPa), with an increase in tensile strength (Rm = 2176 MPa) after austenitization at 900 °C, but at the cost of a reduced yield strength (Rp0.2 = 1561 MPa). The lowest tensile properties (Rm = 2023 MPa, Rp0.2 = 1440 MPa) were found after austenitization at 1200 °C. The highest elongation at break (9.4%) was observed after austenitization at 850 °C, while the lowest (5.8%) occurred at 1000 °C. Impact toughness was lowest in the as-delivered state (17 J/cm²) and highest after austenitization at 850 °C (33 J/cm²).

The lowest abrasion resistance coefficient (kb = 1.32) was observed in the as-delivered state, while the highest (kb = 1.37) was recorded for the steel austenitized at 850 °C. In hard and brittle structures, material loss is primarily caused by micro-cutting, which smoothens the worn surface, while micro-plowing predominates in less hard, more ductile samples. As the heat treatment temperature increases, the penetrating effect of abrasive grains intensifies, resulting in wider and deeper indentations and pits surrounded by plastically deformed material. The analysis of the

relationships between the microstructural properties, represented by PAGS, and the mechanical properties of Hardox Extreme steel revealed that these properties can be approximated using second-degree polynomials, with determination coefficients ranging from 0.6173 to 0.9420. No strong correlation was found between PAGS and material hardness. However, it was observed that as PAGS increases, the intensity of weight loss also increases, leading to a reduction in abrasion resistance, although the differences in the kb coefficient values are relatively small. The strongest correlation was found for impact toughness, where the determination coefficient reached 0.942, with the function achieving its minimum at an austenitization temperature of 1100 °C.

REFERENCES

1. Konat Ł. Structural aspects of execution and thermal treatment of welded joints of Hardox Extreme steel. Metals (Basel) 2019; 9: 915. https://doi.org/10.3390/met9090915.
2. Białobrzeska B, Jasiński R, Konat L, Szczepański L. Analysis of the properties of Hardox Extreme steel and possibilities of its applications in machinery. Metals (Basel) 2021; 11: 162. https://doi.org/10.3390/met11010162.
3. Zemlik M, Konat Ł, Leśny K, Jamroziak K. Comparison of abrasive wear resistance of Hardox steel and Hadfield cast steel. Applied Sciences 2024; 14: 11141. https://doi.org/10.3390/APP142311141.
4. Zemlik Martyna, Konat Łukasz, Białobrzeska Beata. Analysis of the possibilities to increase abrasion resistance of welded joints of Hardox Extreme steel. Tribol Int 2025; 201. https://doi.org/10.1016/j.triboint.2024.110271.
5. Konat Ł, Pękalski G. Overview of materials testing of brown-coal mining machines (years 1985–2017). In: Sokolski M, editor. Mining Machines and Earth-Moving Equipment, Cham: Springer 2020; 21–58.
6. Konat Ł, Napiórkowski J. The effect of the method and parameters of the heat treatment on abrasive wear resistance of 38GSA steel. Quarterly Tribologia 2019; 2: 61–9. https://doi.org/10.5604/01.3001.0013.5435.
7. Ojala N, Valtonen K, Heino V, Kallio M, Aaltonen J, Siitonen P, et al. Effects of composition and microstructure on the abrasive wear performance of quenched wear resistant steels. Wear 2014; 317: 225–32. https://doi.org/10.1016/J.WEAR.2014.06.003.
8. Mondal J, Das K, Das S. An investigation of mechanical property and sliding wear behaviour of 400Hv grade martensitic steels. Wear 2020; 458–459: 203436. https://doi.org/10.1016/j.wear.2020.203436.
9. Białobrzeska B, Konat Ł. Comparative analysis of abrasive-wear resistance of Brinar and Hardox steels. Tribologia 2017; 272: 7–16. https://doi.org/10.5604/01.3001.0010.6261.
10. Wyrzykowski JW, Pleszakow E, Sieniawski J. Deformation and cracking of metals. Warsaw: Publishing House "WNT"; 1999.
11. Lindroos M, Valtonen K, Kemppainen A, Laukkanen A, Holmberg K, Kuokkala V-T. Wear behavior and work hardening of high strength steels in high stress abrasion. Wear 2015; 322–323: 32–40. https://doi.org/10.1016/j.wear.2014.10.018.
12. Ratia V, Rojacz H, Terva J, Valtonen K, Badisch E, Kuokkala V-T. Effect of multiple impacts on the deformation of wear-resistant steels. Tribol Lett 2015; 57: 15. https://doi.org/10.1007/s11249-014-0460-7.
13. Valtonen K, Ojala N, Haiko O, Kuokkala V-T. Comparison of various high-stress wear conditions and wear performance of martensitic steels. Wear 2019; 426–427: 3–13. https://doi.org/10.1016/j.wear.2018.12.006.
14. Morito S, Tanaka H, Konishi R, Furuhara T, Maki T. The morphology and crystallography of lath martensite in Fe-C alloys. Acta Mater 2003; 51: 1789–99. https://doi.org/10.1016/S1359-6454(02)00577-3.
15. Wang C, Wang M, Shi J, Hui W, Dong H. Effect of microstructure refinement on the strength and toughness of low alloy martensitic steel. J Mater Sci Technol 2007; 23: 659–64.
16. Prawoto Y, Jasmawati N, Sumeru K. Effect of prior austenite grain size on the morphology and mechanical properties of martensite in medium carbon steel. J Mater Sci Technol 2012; 28: 461–6. https://doi.org/10.1016/S1005-0302(12)60083-8.
17. Morris JW. The influence of grain size on the mechanical properties of steel. In: Takaki S, Maki T, editors. In Proceedings of the International Symposium on Ultrafine Grained Steels, Fukuoka, Japan: Iron and Steel Institute of Japan 2001; 34–41. https://doi.org/10.2172/861397.
18. Haiko O, Javaheri V, Valtonen K, Kaijalainen A, Hannula J, Kömi J. Effect of prior austenite grain size on the abrasive wear resistance of ultra-high strength martensitic steels. Wear 2020; 454–455: 203336. https://doi.org/10.1016/j.wear.2020.203336.
19. Hidalgo J, Santofimia MJ. Effect of prior austenite grain size refinement by thermal cycling on the microstructural features of as-quenched lath martensite. Metall Mater Trans A Phys Metall Mater Sci 2016; 47: 5288–301. https://doi.org/10.1007/S11661-016-3525-4/FIGURES/12.
20. Maki T. Morphology and substructure of martensite in steels. Phase Transformations in Steels 2012; 34–58.

https://doi.org/10.1533/9780857096111.1.34.

21. Swarr T, Krauss G. The effect of structure on the deformation of as-quenched and tempered martensite in an Fe-0.2 pct C alloy. Metallurgical Transactions A 1976; 7: 41–8. https://doi.org/10.1007/BF02644037.
22. Wang C, Wang M, Shi J, Hui W, Dong H. Effect of microstructural refinement on the toughness of low carbon martensitic steel. Scr Mater 2008; 58: 492–5. https://doi.org/10.1016/j.scriptamat.2007.10.053.
23. Białobrzeska B, Konat Ł, Jasiński R. The influence of austenite grain size on the mechanical properties of low-alloy steel with boron. Metals (Basel) 2017; 7. https://doi.org/10.3390/met7010026.
24. Dobrzański LA. Podstawy nauki o materiałach i metaloznawstwo. Warszawa: Wydawnictwa Naukowo-Techniczne; 2003.
25. Burakowski T, Wierzchoń T. Inżynieria powierzchni metali. Warszawa: Wydawnictwa Naukowo-Techniczne; 1995.
26. Pawlak K, Białobrzeska B, Konat Ł. The influence of austenitizing temperature on prior austenite grain size and resistance to abrasion wear of selected low-alloy boron steel. Archives of Civil and Mechanical Engineering 2016; 16. https://doi.org/10.1016/j.acme.2016.07.003.
27. Sundström A, Rendón J, Olsson M. Wear behaviour of some low alloyed steels under combined impact/abrasion contact conditions. Wear 2001; 250: 744–54. https://doi.org/10.1016/S0043-1648(01)00712-8.
28. Kömi J, Karjalainen P, Porter D. Direct-quenched structural steels. In: Colás R, Totten GE, editors. Encyclopedia of iron, steel their alloy, Boca Raton: CRC Press 2016; 1109–25. https://doi.org/10.1081/E-EISA-120049737.
29. Hanamura T, Torizuka S, Tamura S, Enokida S, Takechi H. Effect of austenite grain size on transformation behavior, microstructure and mechanical properties of 0.1C–5Mn martensitic steel. Institute of Japan International 2013; 53: 2218–25. https://doi.org/10.2355/ISIJINTERNATIONAL.53.2218.
30. Lan HF, Du LX, Li Q, Qiu CL, Li JP, Misra RDK. Improvement of strength-toughness combination in austempered low carbon bainitic steel: The key role of refining prior austenite grain size. J Alloys Compd 2017; 710: 702–10. https://doi.org/10.1016/J.JALLCOM.2017.03.024.
31. Chatterjee S, Bhadeshia HKDH. TRIP-assisted steels: cracking of high-carbon martensite. Materials Science and Technology 2006; 22: 645–9. https://doi.org/10.1179/174328406X86182.
32. Zemlik M, Białobrzeska B, Stachowicz M, Hanszke J. The influence of grain size on the abrasive wear resistance of Hardox 500 steel. Applied Sciences 2024; 14: 11490. https://doi.org/10.3390/APP142411490.
33. Mukhamedov AA. Strength and wear resistance in relation to the austenite grain size and fine structure of the steel. Metal Science and Heat Treatment 1968; 10: 526–8. https://doi.org/10.1007/BF00654357.
34. Białobrzeska B. The influence of boron on the resistance to abrasion of quenched low-alloy steels. Wear 2022; 500–501: 204345. https://doi.org/10.1016/j.wear.2022.204345.
35. Ligier K, Zemlik M, Lemecha M, Konat Ł, Napiórkowski J. Analysis of wear properties of Hardox steels in different soil conditions. Materials 2022; 15: 7622. https://doi.org/10.3390/ma15217622.
36. Dziubek M, Rutkowska-Gorczyca M, Dudziński W, Grygier D. Investigation into changes of microstructure and abrasive wear resistance occurring in high manganese steel X120Mn12 during isothermal annealing and re-austenitisation process. Materials 2022; 15: 2622. https://doi.org/10.3390/ma15072622.
37. Kocańda Stanisław. Fatigue Failure of Metals. Warsaw: Publishing House "WNT"; 1978.
38. Maciejny A. Brittleness of Metals. Katowice: Publishing House "Śląsk"; 1973.
39. Li X, Lu G, Wang Q, Zhao J, Xie Z, Misra RDK, et al. The effects of prior austenite grain refinement on strength and toughness of high-strength low-alloy steel. Metals (Basel) 2021; 12: 28. https://doi.org/10.3390/MET12010028.
40. Li X, Lu G, Wang Q, Zhao J, Xie Z, Misra RDK, et al. The effects of prior austenite grain refinement on strength and toughness of high-strength low-alloy steel. Metals (Basel) 2021; 12: 28. https://doi.org/10.3390/MET12010028.
41. Simm T, Sun L, McAdam S, Hill P, Rawson M, Perkins K. The influence of lath, block and prior austenite grain (pag) size on the tensile, creep and fatigue properties of novel maraging steel. Materials 2017; 10: 730. https://doi.org/10.3390/MA10070730.
42. Abbaszadeh P, Kheirandish S, Saghafian H, Goodarzy M hossein. Effect of austenitizing temperature on mechanical properties of the mixed bainite - martensite microstructure in CrMoV steel. Materials Research 2017; 21: e20170469. https://doi.org/10.1590/1980-5373-MR-2017-0469.
43. Wang J, Enloe C, Singh J, Horvath C. Effect of prior austenite grain size on impact toughness of press hardened steel. SAE International Journal of Materials and Manufacturing 2016; 9: 488–93.
44. Chen J, Zhang W na, Liu Z yu, Wang G dong. The role of retained austenite on the mechanical properties of a low carbon 3Mn-1.5Ni steel. Metall Mater Trans A Phys Metall Mater Sci 2017; 48: 5849–59. https://doi.org/10.1007/S11661-017-4362-9/METRICS.
45. Chintha AR. Metallurgical aspects of steels designed to resist abrasion, and impact-abrasion wear. Materials Science and Technology 2019; 35: 1133–48. https://doi.org/10.1080/02670836.2019.1615669.